

Article

Application of a New Enhanced Deconvolution Method in Gearbox Fault Diagnosis

Junyuan Wang ¹, Jingtai Wang ¹, Wenhua Du ^{1,*} , Jiping Zhang ¹, Zhijian Wang ^{1,2},
Guanjun Wang ^{3,*} and Tao Li ⁴

¹ School of Mechanical Engineering, North University of China, Taiyuan 030051, China; wangyi01161013@163.com (J.W.); wangjingtai0128@163.com (J.W.); zhjp-0000@163.com (J.Z.); wangzhijian1013@163.com (Z.W.)

² School of Mechanical Engineering, Xi'an Jiao Tong University, Xi'an 030619, China

³ Collage of Information Science & Technology, Hainan University, Haikou 570228, China

⁴ Data Information Room, Shanxi Provincial Military Region, Taiyuan 030013, China; 16635133513@163.com

* Correspondence: dwh@nuc.edu.cn (W.D.); wangguanjun@hainanu.edu.cn (G.W.)

Received: 9 October 2019; Accepted: 25 November 2019; Published: 5 December 2019



Abstract: When the mechanical transmission mechanism fails, such as gears and bearings in the gearbox, its vibration signal often appears as a periodic impact. Considering the influence of noise, however, the fault signal is often submerged in the noise, so it is necessary to propose a feasible and effective fault extraction method. MOMEDA (multipoint optimal minimum entropy deconvolution adjusted) overcomes the tedious iterative process of MED (minimum entropy deconvolution) and overcomes the resampling trouble in MCKD (maximum correlated kurtosis deconvolution). It is suitable for dealing with periodic impact signal. Besides, aiming at the poor ability of MOMEDA to capture the deconvolution result of target function in a strong noise environment, this paper proposes an improved MOMEDA gearbox fault feature extraction method. Considering that MOMEDA has poor anti-noise performance and can easily cause misdiagnosis in a strong noisy environment, this paper constructs an autoregressive mean sliding model to improve the noise immunity of MOMEDA. Firstly, the stability of the test signal is judged by the autocorrelation coefficient (ACF) and the partial correlation coefficient (PACF). Secondly, the ARMA (autoregressive moving average) model is constructed and a set of optimal model coefficients are obtained to filter the signal, which greatly improves MOMEDA's ability to capture fault features. Thirdly, the fault feature is extracted by MOMEDA, and the fault information is extracted accurately under a strong noise environment. Finally, compared with AR-MED, ARMAMED, and other methods, the advantages of ARMAMED are verified. Moreover, the effectiveness and superiority of the proposed method are verified by simulation signals and experimental data from the Case Western Reserve University Bearing Data Center.

Keywords: autoregressive moving average model; multipoint optimal minimum entropy deconvolution adjusted; feature extraction; rotating machinery

1. Introduction

When bearing gear, inner ring, outer ring, or rolling element faults occur, the transmission system will be affected and the vibration signal will appear periodically impacted [1–5]. When the bearing faults occur, the background noise becomes loud owing to the gearbox harsh working environment [6–10]. The weak fault signal is often overwhelmed by noise, and it is difficult to extract the characteristic information. Therefore, the weak fault extraction of the rotating machine is still a big challenge [11–14].

The extraction of the fault information is actually to weaken the noise in the collected vibration signals through an optimal filter, which effectively preserves the integrity of the fault

information [15–18]. At present, the existing fault diagnosis methods include time-frequency analysis, mode decomposition [19], sparse theory [20], order tracking [21], fuzzy theory [22], morphology theory [23–25], stochastic resonance [26], intelligent recognition method [27], deconvolution theory, and others. As the noise and fault characteristics in the vibration signals are convolution, the deconvolution of vibration signals can separate the noise and fault information. Minimum entropy deconvolution (MED) is an adaptive system identification method. Its basic principle is to solve the deconvolution so that the results highlight a few sharp pulses, and the maximum kurtosis is used as the iterative termination condition [28].

Sawalhi N [29] first applied MED to the diagnosis of rolling bearing and gear faults in 2007. However, the MED algorithm is susceptible to noise and the maximum kurtosis as the objective function cannot reasonably reflect the continuity of the impact signal [30,31]. In order to overcome the shortcomings of MED, Geoff et al. [32] proposed a fault feature extraction method of rotating machinery, called multi-point optimal minimum entropy deconvolution (MOMEDA). Compared with MED, this method can obtain the optimal filter without iteration. It defines the position and weight of the deconvoluted pulse sequence with the time objective function [33,34]. Every rotation period can be collected with the shock pulse. When the fault period is not an integer, MOMEDA can directly extract the fault without resampling. In addition, owing to the introduction of multi-point kurtosis, the periodic components of fault signals can be calculated, which provides a new idea for the fault feature extraction of rotating machinery [35]. The MOMEDA method proposed by Geoff et al. mainly focuses on the gear fault in the gearbox at the beginning of the fault signal extraction. The fault signal is a strong shock signal, but the fault information extraction performance of MOMEDA is significantly variable under different SNR (signal-to-noise ratio) conditions. In order to ensure the accuracy of MOMEDA algorithm for fault information extraction, it is necessary to improve the anti-noise performance of MOMEDA. Wang, Z.J. et al. [36] successfully extracted the fault features in the wind turbine gearbox by combining MED and MOMEDA, however, the defects of the MED algorithm in iteratively selecting filters cannot be ignored [37,38].

The time series autoregressive (AR) model is widely used in the noise reduction processing of vibration signals. Takalo, R. et al. [39] applied the AR (autoregressive) model to reduce the noise in SPECT (single photon emission computed tomography) images, which compared the filtered signal of an AR filter with a Butterworth filter to verify the advantages of the AR filter in noise reduction. In recent years, AR has been successfully applied to fault diagnosis. H. Endo [40] proposed an autoregressive minimum entropy deconvolution (AR-MED) fault extraction method. Using AR filtering technology is insensitive and can be better to distinguish the performance of noise and pulse, thus improving the fault feature extraction ability of MED; this method can also be used to achieve fault extraction for gear spline and tooth angle crack. On this basis, Qing Li et al. [41] improved the method under the limitations of the autoregressive minimum entropy deconvolution (AR-MED) in a strong noise environment and proposed a method combining autoregressive minimum entropy deconvolution and variational mode decomposition (AR-MED-VMD) to extract the bearing outer ring fault. However, the existing methods only use the AR model, while the parameterized ARMA (autoregressive moving average) model can more accurately describe the objective law of the dynamic system and the accuracy of data processing is better than with the AR model. Gao, S. et al. [42] obtained the relationship between mortar noise, velocity, and concentration by reducing the noise of the slurry by the ARMA model. Therefore, this paper proposes the combination of ARMA and MOMEDA to extract the weak fault features, improve the anti-noise performance of MOMEDA through ARMA, and realize the accurate fault information extraction by MOMEDA in a strong noise environment. The feasibility of this method is verified by the simulation and the experiment.

2. Basic Theory

2.1. MOMEDA Method

MED can only extract a single pulse. In order to improve this defect, Geoff L. proposed maximum correlated kurtosis deconvolution (MCKD), but the length, noise reduction interval, and shift number of the algorithm parameter filter have a great influence on the effect. Furthermore, MCKD can only effectively extract a limited number of pulses, which limits the detection efficiency. Therefore, in 2016, Geoff L. [32] successfully extracts continuous periodic impact by solving the idea of optimal filter by the non-iterative method. Named MOMEDA, the idea of this method is as follows:

Vibration signal collected by the sensor $y(n)$:

$$y(n) = h(n)x(n) + q(n), \tag{1}$$

where $q(n)$ is noise, $x(n)$ is the impact sequence, and $h(n)$ is the transfer function. The purpose of MOMEDA is to obtain an FIR (finite impulse response) filter, making the output $y(n)$ match the original impact signal $x(n)$ to the maximum extent.

MOMEDA is a deconvolution algorithm for multi-pulse identification of signals. In order to obtain continuous impact pulses, the concept of MDN (Multiple D-norm) is introduced in Equation (2), and its maximum value is the minimum entropy deconvolution (MOMEDA) of multi-point optimization in Equation (3):

$$MDN(\vec{y}, \vec{t}) = \frac{1}{\|\vec{t}\|} \frac{\vec{t}^T \vec{y}}{\|\vec{y}\|}. \tag{2}$$

The maximum value is

$$\max_f MDN(\vec{y}, \vec{t}) = \max_f \frac{\vec{t}^T \vec{y}}{\|\vec{y}\|}, \tag{3}$$

where \vec{t} is the target vector for determining the impact pulse position; f is the filter coefficient; and $t = t_1, t_2, \dots, t_{N-L}$, $f = f_1, f_2, \dots, f_L$. The target solution will change with the sampling frequency, and different period pulses can be extracted at the same sampling frequency. Simultaneously, the target vector \vec{t} can effectively identify fault information and noise.

The extremum of Equation (3) can be obtained by deriving the filter coefficient:

$$\frac{d}{df} \left(\frac{\vec{t}^T \vec{y}}{\|\vec{y}\|} \right) = \frac{d}{df} \frac{t_1 y_1}{\|\vec{y}\|} + \frac{d}{df} \frac{t_2 y_2}{\|\vec{y}\|} + \dots + \frac{d}{df} \frac{t_{N-L} y_{N-L}}{\|\vec{y}\|}, \tag{4}$$

because $\frac{d}{df} \frac{t_k y_k}{\|\vec{y}\|} = \|\vec{y}\|^{-1} t_k \vec{M}_k - \|\vec{y}\|^{-3} t_k y_k X_0 \vec{y}$, and $\vec{M}_k = \begin{bmatrix} x_{k+L-1} \\ x_{k+L-2} \\ \vdots \\ x_k \end{bmatrix}$.

Therefore, Equation (4) can be written as follows:

$$\frac{d}{df} \left(\frac{\vec{t}^T \vec{y}}{\|\vec{y}\|} \right) = \|\vec{y}\|^{-1} (t_1 \vec{M}_1 + t_2 \vec{M}_2 + \dots + t_{N-L} \vec{M}_{N-L}) - \|\vec{y}\|^{-3} \vec{t}^T \vec{y} X_0 \vec{y}. \tag{5}$$

The simplified result is the following:

$$t_1 \vec{M}_1 + t_2 \vec{M}_2 + \dots + t_{N-L} \vec{M}_{N-L} = X_0 \vec{t}. \tag{6}$$

Let Equation (5) equal 0 and it will become the following:

$$\|\vec{y}\|^{-1} X_0 \vec{t} - \|\vec{y}\|^{-3} \vec{t} \vec{y} X_0 \vec{y} = \vec{0},$$

which is $\frac{\vec{t} \vec{y}}{\|\vec{y}\|^2} X_0 \vec{y} = X_0 \vec{t}$.

Because $\vec{y} = X_0^T \vec{f}$ and the assumption $(X_0 X_0^T)^{-1}$ exists,

$$\frac{\vec{t} \vec{y}}{\|\vec{y}\|^2} \vec{f} = (X_0 X_0^T)^{-1} X_0 \vec{t}. \tag{7}$$

The MOMEDA filter and output solution can be summarized as follows:

$$\vec{f} = (X_0 X_0^T)^{-1} X_0 \vec{t}, \tag{8}$$

$$X_0 = \begin{bmatrix} x_L & x_{L+1} & x_{L+2} & \cdots & \cdots & x_N \\ x_{L-1} & x_L & x_{L+1} & \cdots & \cdots & x_{N-1} \\ x_{L-2} & x_{L-1} & x_L & \cdots & \cdots & x_{N-2} \\ \vdots & \vdots & \vdots & \ddots & \cdots & \vdots \\ x_1 & x_2 & x_3 & \cdots & \cdots & x_{N-L+1} \end{bmatrix}_{L \text{ by } N-L+1}, \tag{9}$$

$$\vec{y} = X_0^T \vec{f}. \tag{10}$$

As the multiple of the filter is the solution of Equation (10), the multiple of $\vec{f} = (X_0 X_0^T)^{-1} X_0 \vec{t}$ is the solution to the MOMEDA problem. This method completely avoids the effect of iterative operations and periodicity on the noise reduction effect of integers.

2.2. ARMA Method

The parametric ARMA model can accurately describe the objective laws of dynamic systems. The autoregressive parameters are most sensitive to the changes in working conditions and have obvious advantages in small damage identification, noise reduction, and operability. In general, the time series required for prediction is a stationary time series, which is also a precondition for the differential autoregressive moving average model. In reality, most sequences are non-stationary sequences. Therefore, it is smoothed by appropriate differentiation of the sequence or logarithmic transformation, and then the differential autoregressive moving average model is used for modeling.

The general formula of the autoregressive moving average model $ARMA(n, m)$ can be expressed as follows:

$$x_t = \sum_{i=1}^n \varphi_i x_{t-i} + \alpha_t - \sum_{j=1}^m \theta_j \alpha_{t-j}, \tag{11}$$

where n is the autoregressive order; m is the moving average order; $\varphi_i (i = 1, 2, \dots, n)$ is the autoregressive parameter; $\theta_j (j = 1, 2, \dots, m)$ is the moving average parameter; and α_t is a Gaussian white noise process with a mean of 0 and a variance of σ_α^2 .

The $ARMA(n, m)$ model has the tailing properties of both the autocorrelation coefficient and the partial autocorrelation coefficient. Trailing means that, as the independent variable k increases indefinitely, the function value tends to 0 at a negative exponential speed. When $m = 0$, the $ARMA(n, m)$ model degenerates into the $AR(n)$ model. When $n = 0$, the $ARMA(n, m)$ model degenerates into the $MA(m)$ model. The choice of ARMA for the prediction of vibration data of rolling bearings is to analyze the partial autocorrelation coefficient and autocorrelation coefficient of the sample to be tested,

so as to select the appropriate model to fit the sequence to be tested, and finally use the information criterion to test the applicability of the model.

The simple correlation between each sequence value $x_t, x_{t-1}, \dots, x_{t-k}$ that makes up the time series is called autocorrelation.

The autocorrelation coefficient γ_k can be used to measure the degree of autocorrelation. k is a time interval.

$$\gamma_k = \frac{E[x_t x_{t+k}]}{E[x_t^2]} = \frac{\sum_{t=1}^{a-k} (x_t - \bar{x})(x_{t+k} - \bar{x})}{\sum_{t=1}^a (x_t - \bar{x})^2}, \tag{12}$$

where a is the sample size, k is the period of lag, and \bar{x} is the sample average mean. It is known from Schwarz's inequality $E[xy] \leq \sqrt{E[x^2]E[y^2]}$ that $[-1, 1]$ is the value field of the autocorrelation coefficient γ_k , and the absolute value of the autocorrelation coefficient is close to 1, the degree of autocorrelation is higher.

Partial autocorrelation is defined as time series X_t , which indicates the conditional correlation between time series values under certain conditions. The partial autocorrelation coefficient φ_{kk} is used to measure its correlation, and the value range φ_{kk} is $[-1, 1]$.

$$\left\{ \begin{array}{l} \gamma_1 \\ \gamma_k - \sum_{j=1}^{k-1} \varphi_{k-1,j} \gamma_{k-j} \\ \frac{\gamma_k - \sum_{j=1}^{k-1} \varphi_{k-1,j} \gamma_{k-j}}{1 - \sum_{j=1}^{k-1} \varphi_{k-1,j} \gamma_j} \end{array} \right. \tag{13}$$

The AIC (Akaike's Information Criterion) criterion extracts the maximum amount of information in the observation sequence and, from this point on, is suitable for testing the ARMA (n, m) model order.

The criteria function is defined as follows:

$$AIC(p) = -2 \ln L + 2p, \tag{14}$$

where $p = m + n$, L is the likelihood function of the time series x_t ; if the time series x_t is stationary and normal, then

$$L = \prod_{t=1}^N \frac{1}{\sqrt{2\pi}\sigma_a} \exp\left[-\frac{1}{2\sigma_a^2} (x_t - \hat{\mu}_t)^2\right], \tag{15}$$

where $\hat{\mu}_t$ is the mathematical expectation estimate of x_t whose time is t , that is, $E[x_t]$. Then, by substituting $x_t - \hat{\mu}_t = a_t$ into the above formula and performing the multiplication calculation, Formula (16) is obtained.

$$L = \left(\frac{1}{2\pi\sigma_a^2}\right)^{\frac{N}{2}} \exp\left[-\frac{1}{2\sigma_a^2} \sum_{t=1}^N a_t^2\right], \tag{16}$$

where σ_a^2 is calculated as follows:

$$\sigma_a^2 = \frac{1}{N} \sum_{t=1}^N a_t^2. \tag{17}$$

Substituting Equation (17) into Equation (16) and taking the natural logarithm on both sides of the equal sign, there are the following:

$$\ln L = -\frac{N}{2} (\ln 2\pi + \ln \sigma_a^2) - \frac{N}{2}, \tag{18}$$

which is

$$-2 \ln L = N \ln 2\pi + N \ln \sigma_a^2 + N. \tag{19}$$

Substituting Equation (19) into Equation (13), for a given data type, the length is N , and the latter two of Equation (19) are constant, which has no effect on the comparison result of $AIC(p)$ and can be omitted, thus obtaining the following:

$$AIC(p) = N \ln \sigma_a^2 + 2p. \tag{20}$$

Obviously, given a model parameter estimation method, $AIC(p)$ is a function of p . If p increases, then $\ln \sigma_a^2$ decrease, but the latter $2p$ increases. Therefore, the model order p when the value of $AIC(p)$ is the smallest is the applicable model order.

After the order of the ARMA model is determined, the parameters in AR and MA should be estimated. In this paper, sequence estimation method is used in the simultaneous order theory estimation method to first estimate φ_i , and then estimate θ_j .

It can be known from the recursive formula of R_k that, when $k > m$, the formula of R_k will not contain θ_j .

$$R_k = \varphi_1 R_{k-1} + \varphi_2 R_{k-2} + \dots + \varphi_n R_{k-n} (k > m) \tag{21}$$

Note the subscript of R_k in the above equation. When $k < 0$, as R_k is the property of the even function, there is $R_{-k} = R_k$, separately $k = m + 1, \dots, m + n$, the following matrix equation can be seen:

$$\begin{bmatrix} R_{m+1} \\ R_{m+2} \\ \dots \\ R_{m+n} \end{bmatrix} = \begin{bmatrix} R_m & R_{m-1} & R_{m-2} & \dots & R_{m-n+1} \\ R_{m+1} & R_m & R_{m-1} & \dots & R_{m-n+2} \\ \dots & \dots & \dots & \dots & \dots \\ R_{m+n-1} & R_{m+n-2} & R_{m+n-3} & \dots & R_m \end{bmatrix} \begin{bmatrix} \varphi_1 \\ \varphi_2 \\ \dots \\ \varphi_n \end{bmatrix}. \tag{22}$$

If both sides of the equation are divided by R_0 , then each R_k in the equation is transformed into the autocorrelation coefficient ρ_k . This equation is the modified Yule–Walker equation, which can be abbreviated as follows:

$$R_A = R_B \varphi. \tag{23}$$

In Equation (23), R_A is the n -dimensional column vector to the left of the matrix equation, R_B is the n -order order square matrix to the right of the matrix equation, and φ is a n -dimensional column vector composed of autoregressive coefficients. This matrix is not a Toeplitz matrix, but generally has an inverse matrix, so the matrix equation can be solved, and the estimated value of the autoregressive parameter is as follows:

$$\varphi = R_B^{-1} R_A. \tag{24}$$

At this point, the autoregressive parameters $\varphi_i (i = 1, 2, \dots, n)$ of the ARMA model have been determined.

In the ARMA model in Equation (11), let $y_t = x_t - \sum_{i=1}^n \varphi_i x_{t-i}$, then $y_t = a_t - \sum_{j=1}^m \theta_j a_{t-j}$.

This can also be recorded as follows:

$$\begin{aligned} y_t &= - \sum_{i=0}^n \varphi_i x_{t-i} (\varphi_0 = -1) \\ y_t &= - \sum_{j=0}^m \theta_j a_{t-j} (\theta_0 = -1) \end{aligned} \tag{25}$$

Multiply both sides of the AR model of Equation (25) by y_{t-k} and find the mathematical expectation, there is

$$R_{y,k} = E \left[\sum_{i=0}^n \varphi_i x_{t-i} \sum_{j=0}^n \varphi_j x_{t-k-j} \right] = \sum_{i=0}^n \sum_{j=0}^n \varphi_i \varphi_j E[x_{t-i} x_{t-k-j}] = \sum_{i=0}^n \sum_{j=0}^n \varphi_i \varphi_j R_{k+j-i} \tag{26}$$

where R_{k+j-i} is the autocorrelation function of the observation time series $\{x_t\}$,

$$R_k = \frac{1}{N} \sum_{t=k+1}^N x_t x_{t-k} \quad (k = 0, 1, 2, \dots, N - 1). \tag{27}$$

Similarly, the MA model of Equation (25) has

$$R_{y,k} = E \left[\sum_{i=0}^m \theta_i a_{t-i} \sum_{j=0}^m \theta_j a_{t-k-j} \right] = \sum_{i=0}^m \sum_{j=0}^m \theta_i \theta_j a_{t-i} a_{t-k-j} = \sum_{i=0}^m \sum_{j=0}^m \theta_i \theta_j \sigma_a^2 \delta_{k+j-i}, \tag{28}$$

which is

$$R_{y,k} = \sigma_a^2 \sum_{j=0}^m \theta_j \theta_{j+k}. \tag{29}$$

For the MA model of Equation (29), the B operator polynomial $\varphi(B) = 1$ in the autoregressive part, then the spectral density function $S_{yy}(\omega)$ is as follows:

$$S_{yy}(\omega) = \sigma_a^2 \left| \frac{\theta(B)}{\varphi(B)} \right|_{B=e^{-i\omega\Delta}}^2 = \sigma_a^2 |\theta(B)|_{B=e^{-i\omega\Delta}}^2. \tag{30}$$

In Equation (30), in the moving average part, $\theta(B)$ is a B operator polynomial, and if the characteristic root of the MA part is denoted by η_i , then

$$S_{yy}(\omega) = \sigma_a^2 \left| \prod_{j=1}^m (1 - \eta_j B) \right|_{B=e^{-i\omega\Delta}}^2. \tag{31}$$

Obviously, when $B = 1/\eta_j$, $S_{yy}(\omega) = 0$. On the other hand, according to the definition of the spectral density function,

$$S_{yy}(\omega) = F[R_{y,k}] = \sum_{k=-\infty}^{\infty} R_{y,k} B^k \Big|_{B=e^{-i\omega\Delta}}. \tag{32}$$

It is known from Equation (29) that, as the subscript j of the model parameter θ_j can only change range $(0, m)$, when $j > m$, $\theta_j = 0$, and thus the subscript k of $R_{y,k}$ varies in the range of $(0, m)$, otherwise $R_{y,k} = 0$. Therefore, the sum of the Fourier transforms in this equation can be written as follows:

$$S_{yy}(\omega) = \sum_{k=0}^{\infty} R_{y,k} B^k \Big|_{B=e^{-i\omega\Delta}}. \tag{33}$$

This formula should be equal to Equation (31), so when $B = 1/\eta_j$, there should be

$$\sum_{k=0}^m R_{y,k} \left(\frac{1}{\eta_j}\right)^k = 0, \tag{34}$$

which is

$$R_{y,0} + R_{y,1} \frac{1}{\eta_j} + R_{y,2} \left(\frac{1}{\eta_j}\right)^2 + \dots + R_{y,m} \left(\frac{1}{\eta_j}\right)^m = 0. \tag{35}$$

This formula is a one-dimensional m -order equation for $1/\eta_j$, then m roots $1/\eta_j (j = 1, 2, \dots, m)$ can be solved by this formula; then, η_j is substituted into the polynomial.

$$\theta(B) = \prod_{j=1}^m (1 - \eta_j B) = 1 - \sum_{j=1}^m \theta_j B^j \quad (36)$$

Comparing the same power factor of the B operator can get θ_j .

At this point, the sliding average parameter $\theta_j (j = 1, 2, \dots, m)$ of the ARMA model has been determined.

The ARMA forecasting process is as follows:

Step 1: Determine the stationarity of the test sequence. If the test sample is an unstable sequence, the sequence is subjected to a differential operation to transform it into a stationary random sequence, and then subjected to an averaging process;

Step 2: Calculate the autocorrelation coefficient (ACF) and the partial correlation coefficient (PACF) of the test sequence after the differential operation, and judge the stationarity again;

Step 3: Calculate the parameter values of the model using the least-squares method, and use the AIC criterion to determine the order;

Step 4: Test the obtained model and make a reasonable optimization;

Step 5: Use the optimal model obtained in the above steps to predict unknown sequence data.

3. Limitations and Improvements of MOMEDA

The MOMEDA algorithm has a good effect in the extraction of periodic fault features. The algorithm can obtain the optimal filter without iteration and can extract continuous pulses, but it also has certain limitations. For example, noise has a great influence on it, and it is not ideal to extract weak shock signal under normal working conditions. Aiming at this limitation of the MOMEDA fault extraction method, this paper proposes a fault diagnosis method based on ARMA-MOMEDA. The parametric ARMA model can accurately describe the objective law of the dynamic system; the autoregressive parameters are most sensitive to the change of working conditions, and have obvious advantages in small damage identification, noise reduction, and operability. By building an autoregressive moving average model for fault signals, a set of optimal models is obtained. The model is used to filter the fault signal and separate the uncorrelated impact components. Therefore, ARMA is used as a pre-filter of MOMEDA to denoise the signal to improve the limitation of MOMEDA in extracting fault features in a strong noise environment.

3.1. Limitations of the MOMEDA Method

In the single fault diagnosis, MOMEDA has certain limitations in the extraction of weak faults. The periodic impact it finds may be false components and cannot be accurately identified for fault features [33–35].

To illustrate the impact of different noise on MOMEDA performance, an analog signal is constructed, as shown in Equation (37), for comparison.

$$\begin{aligned} x_1(t) &= A_m \times \exp\left(-\frac{g}{T_m}\right) \sin(2\pi f_a t) \\ x_2(t) &= x_1(t) + \text{noise} \end{aligned} \quad (37)$$

where $x(t)$ is the periodic impact signal, A_m is the amplitude of the impact, g is the damping coefficient, T_m is the period of the impact, and f_a is the natural frequency of the shaft. The parameter is set to the following: $g = 0.1$, $T_m = 0.02$ s, $f_a = 320$ Hz.

In order to further verify the effect of noise on MOMEDA extraction faults, different noise sizes are selected for simulation analysis. The extraction effect of MOMEDA is shown in Figures 1–3. It can be seen from the Figures 1–3 that, as the signal-to-noise ratio decreases, the 50 Hz shock period is gradually submerged by noise. In Figure 1d or Figure 2d, the fault period ($T = 50$) can also be extracted,

but as the signal-to-noise ratio decreases again, the fault period in the envelope spectrum in Figure 3d cannot be extracted accurately. Figure 1a is the simulated bearing fault impact signal. Figure 1b is the noise of 7.76 dB, Figure 1c shows the signal diagram with 7.76 dB noise added, Figure 1d shows the MOMEDA extracts the result when 7.76 dB noise is added, and Figure 1e shows the results of the envelope spectrum. Figure 2a is the simulated bearing fault impact signal, Figure 2b is the noise of 1.74 dB, Figure 2c shows the signal diagram with 1.74 dB noise added, Figure 2d shows the MOMEDA extracts the result when 1.74 dB noise is added, and Figure 2e shows the results of the envelope spectrum. Figure 3a is the simulated bearing fault impact signal, Figure 3b is the noise of -3.11 dB, Figure 3c shows the signal diagram with -3.11 dB noise added, Figure 3d shows the MOMEDA extracts the result when -3.11 dB noise is added, and Figure 3e shows the results of the envelope spectrum.

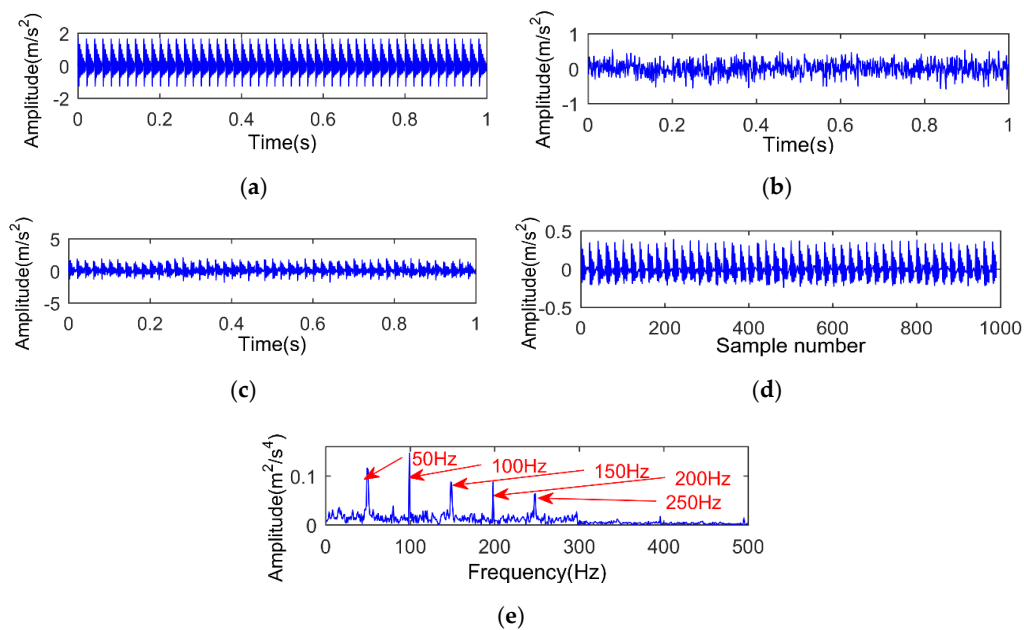


Figure 1. Multipoint optimal minimum entropy deconvolution adjusted (MOMEDA) extraction rendering when 7.76 dB noise is added. (a) The fault signal; (b) the noise of 7.76 dB; (c) a composite signal of noise and fault signal; (d) MOMEDA extracts the result when 7.76 dB noise is added; (e) envelope spectrum after fault extraction when 7.76 dB noise is added.

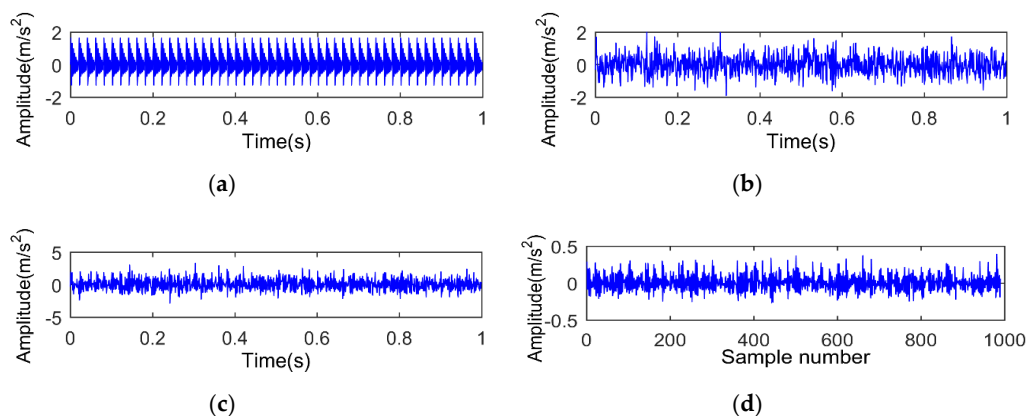


Figure 2. Cont.

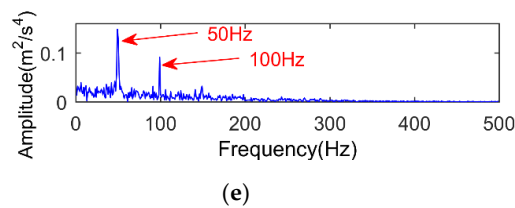


Figure 2. MOMEDA extraction rendering when 1.74 dB noise is added. (a) The fault signal; (b) the noise of 1.74 dB; (c) a composite signal of noise and fault signal; (d) MOMEDA extracts the result when 1.74 dB noise is added; (e) envelope spectrum after fault extraction when 1.74 dB noise is added.

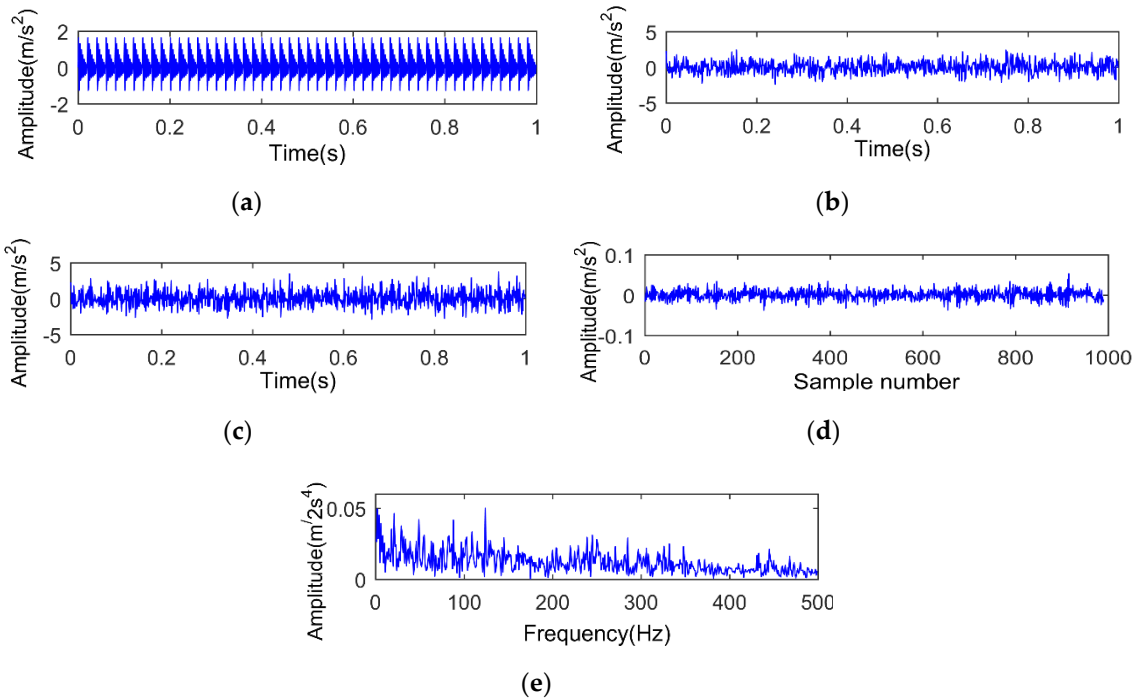


Figure 3. MOMEDA extraction rendering when -3.11 dB noise is added. (a) The fault signal; (b) the noise of -3.11 dB; (c) a composite signal of noise and fault signal; (d) MOMEDA extracts the result when -3.11 dB noise is added; (e) envelope spectrum after fault extraction when -3.11 dB noise is added.

3.2. Based on Improved MOMEDA Fault Diagnosis Method

On the basis of the limitations of the MOMEDA method in the gearbox fault diagnosis process, the ARMA-MOMEDA method proposed in this paper is used to extract the gearbox fault to verify the rationality of this method. Because MOMEDA cannot identify the fault feature in the noisy environment, and the periodic impact component of the characterizing bearing fault is less correlated with other components in signal, the ARMA model estimated by the autocorrelation function is used for filtering, the periodic impact component in the fault signal can be effectively separated from other unrelated components. After ARMA filtering, the fault signal is mainly composed of a highly correlated periodic impact component and partial noise. The flow chart of the ARMA-MOMEDA method is shown in Figure 4. The method steps are as follows:

Step 1: Detect signal stability. Firstly, the inverse order test is used to judge the stationarity of the signal. If it is not stable, the d-differential operation is used to enhance the stationarity.

Step 2: Use the autocorrelation coefficient (ACF) and partial autocorrelation coefficient (PACF) spectra to judge the signal stationarity again.

Step 3: Given the selection range of (n, m) and estimating the parameters φ_i and θ_i of the ARMA (n, m) model.

Step 4: Use the AIC criteria to determine the order of ARMA (n, m) .

Step 5: After the signal is denoised by the fixed-stage ARMA filter, the fault is extracted using MOMEDA.

Step 6: For multi-fault diagnosis, first use the multi-point kurtosis theory to divide the fault extraction interval of the ARMA noise-reduced signal. The MOMEDA filter is used in sequence for the feature extraction.

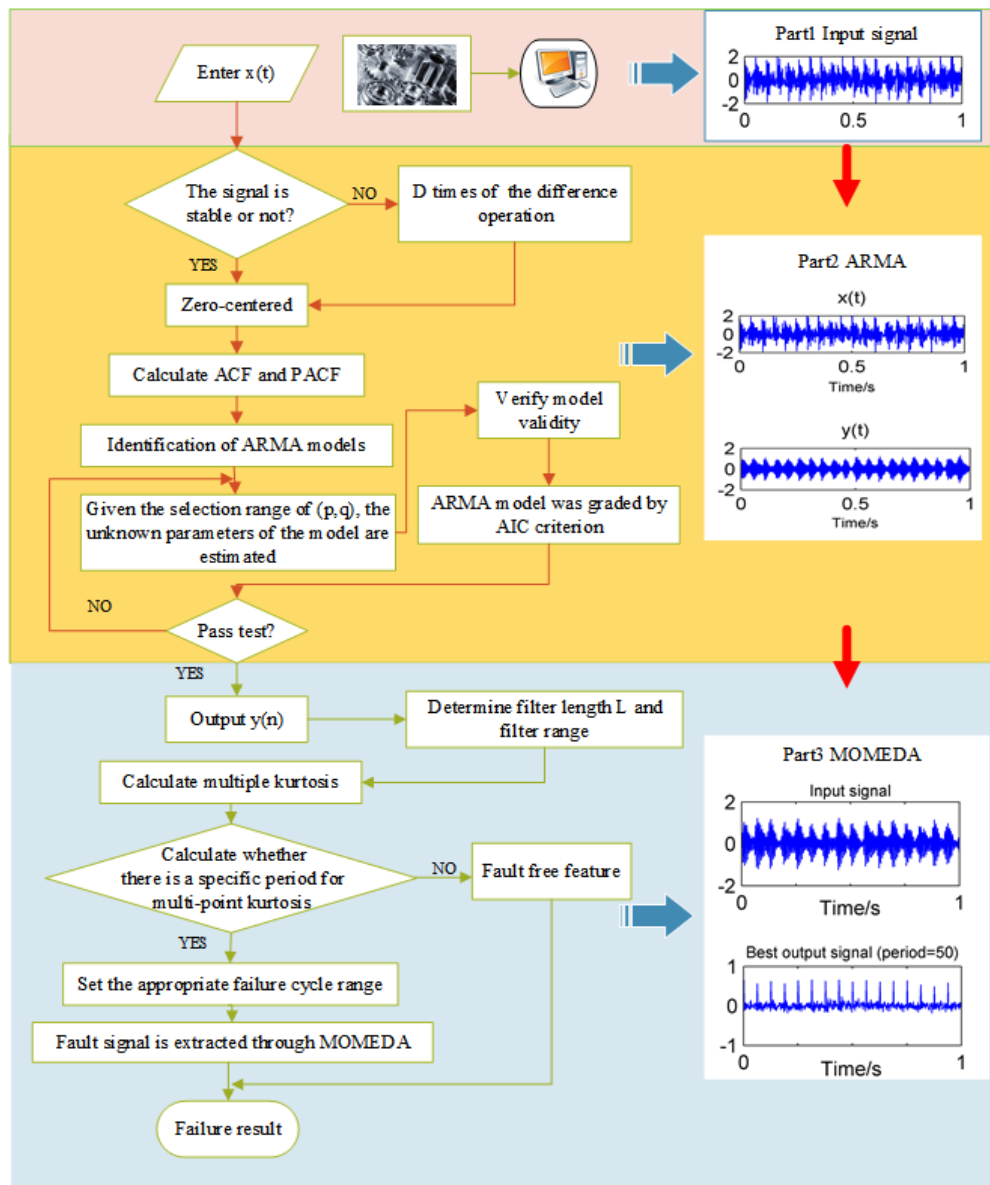


Figure 4. The flow chart of autoregressive moving average (ARMA)-MOMEDA method. ACF, autocorrelation coefficient; PACF, partial correlation coefficient.

4. Simulation Verification

In order to verify the effectiveness and superiority of the proposed method, the following signals were constructed for simulation experiments. The vibration signal of the bearing fault is usually expressed as a periodic impact. The model is shown in Equation (38):

$$\begin{aligned}
 x_1(t) &= A_m \times \exp\left(-\frac{\delta}{T_m}\right) \sin(2\pi f_a t) \\
 x_2(t) &= x_1(t) + \text{noise}
 \end{aligned}
 \tag{38}$$

where $x(t)$ is the periodic impact signal, A_m is the amplitude of the impact, g is the damping coefficient, T_m is the period of the impact, and f_a is the natural frequency. The parameter is set as follows: $g = 0.2$, $T_m = 0.025$ s, $f_a = 320$ Hz. The resulting fault frequency is $1/T_m = 40$ Hz. Figure 5 shows the time domain waveform of the simulated signal. Figure 5a is the simulated bearing fault impact signal. Figure 5b is the noise of -4.36 dB. Figure 5c shows the signal diagram with -4.36 dB noise added. It can be seen that the impact signal shown in Figure 5a simulating the bearing fault is submerged by random noise, and no periodic impact is observed in the composite signal, shown in Figure 5c.

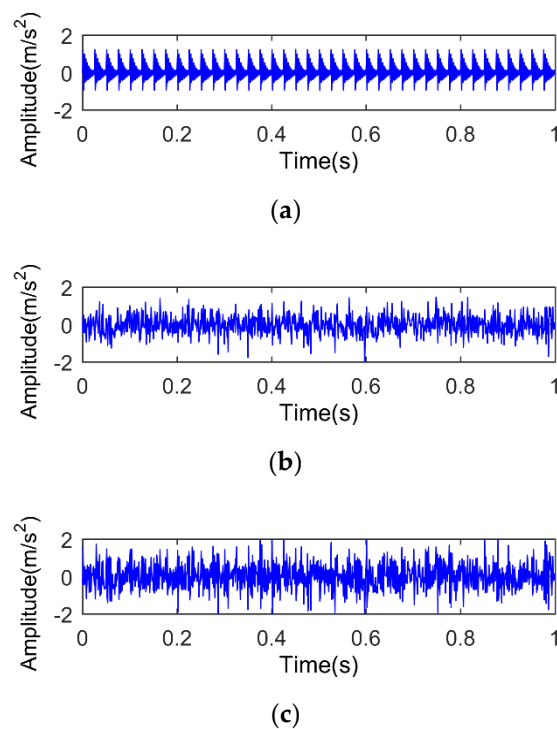


Figure 5. Simulation signal time-domain diagram. (a) The fault signal; (b) the noise of -4.36 dB; (c) a composite signal of noise and fault signal.

In order to fully illustrate the superiority of ARMA-MOMEDA, the above simulation signals are processed by the AR filter [43], ARMA filter [44], MED filter [38], AR-MED [41], ARMA-MED, and ARMA-MOMEDA; Envelope analysis is performed on the processed result to obtain an envelope spectrum, so that the effects of each method were fully compared.

Figure 6 shows the results obtained by the respective methods. Figure 6a is a time-domain diagram and a frequency-domain diagram after AR filter processing. From the time domain diagram, it can be seen that the signal can be noise-reduced, and the partially submerged shock signal appears in the time-domain waveform, but the impact has no obvious periodicity. In the envelope spectrum results, the spectral lines are also cluttered, and the spectral lines corresponding to the obvious faults are not resolved. Therefore, in a noisy environment, AR cannot accurately diagnose the fault frequency.

Figure 6b is a time-domain diagram and a frequency-domain diagram after ARMA filter processing. From the time-domain diagram, it can be seen that the impact that is submerged by noise appears, and the impact has a certain periodicity. The envelope spectrum also shows the spectral line of the fault characteristic frequency. It can be seen that the ARMA result is better than the AR result. However, a large amount of noise can still be observed from the time-domain map, and the periodic impact is not obvious. However, although the frequency corresponding to the fault appears in the envelope spectrum, there are fewer spectral lines and the fault characteristics are not obvious. If you increase the noise, ARMA will also not detect the fault information.

Figure 6c is a time-domain diagram and a frequency-domain diagram after MED filter processing. The impact of being submerged by noise appeared from the time-domain diagram, but no periodicity was observed. The frequency of the fault can be observed in the envelope spectrum, but there is no multiplier and there is a lot of noise. It can be seen that the MED extraction results are better than the AR filter, but not as good as the ARMA filter results.

Figure 6d is a time-domain diagram and a frequency-domain diagram after AR-MED filter processing. In the time-domain diagram, the impact of being submerged by noise appears, and a certain periodicity can be observed. The envelope spectrum also shows the fault frequency. It can be seen that the results of AR-MED are better than those of AR and MED, and AR-MED can improve AR and MED filters. However, it can be seen from the time-domain diagram that the noise-reduced signal still contains a lot of noise, so that the periodic impact is not obvious. The envelope spectrum also shows only a distinct line, and there is no multiplier.

Figure 6e is a time-domain diagram and a frequency-domain diagram after ARMA-MED filter processing. It can be seen from the time-domain diagram that the impact of noise inundation can be extracted after ARMA-MED filtering. In the envelope spectrum, the fault frequency and double frequency and treble frequency can also be observed. It can be seen that the effect is better than that of AR-MED. However, it can be seen that the envelope spectrum contains a large amount of noise, resulting in an insignificant line.

Figure 6f is a time-domain diagram and a frequency-domain diagram after ARMA-MOMEDA filter processing. It can be seen from the time-domain diagram that the ARMA-MOMEDA filter can extract the impact that is submerged by noise, and the periodicity is obvious, and the noise is smaller than other methods. In the envelope spectrum, the fault frequency and double frequency, treble frequency, and quadruple frequency can also be clearly observed. The amplitude is also larger than the amplitude of ARMA-MED, and the noise in the envelope spectrum is much smaller than that of ARMA-MED, which shows that the effect is better than that of ARMA-MED.

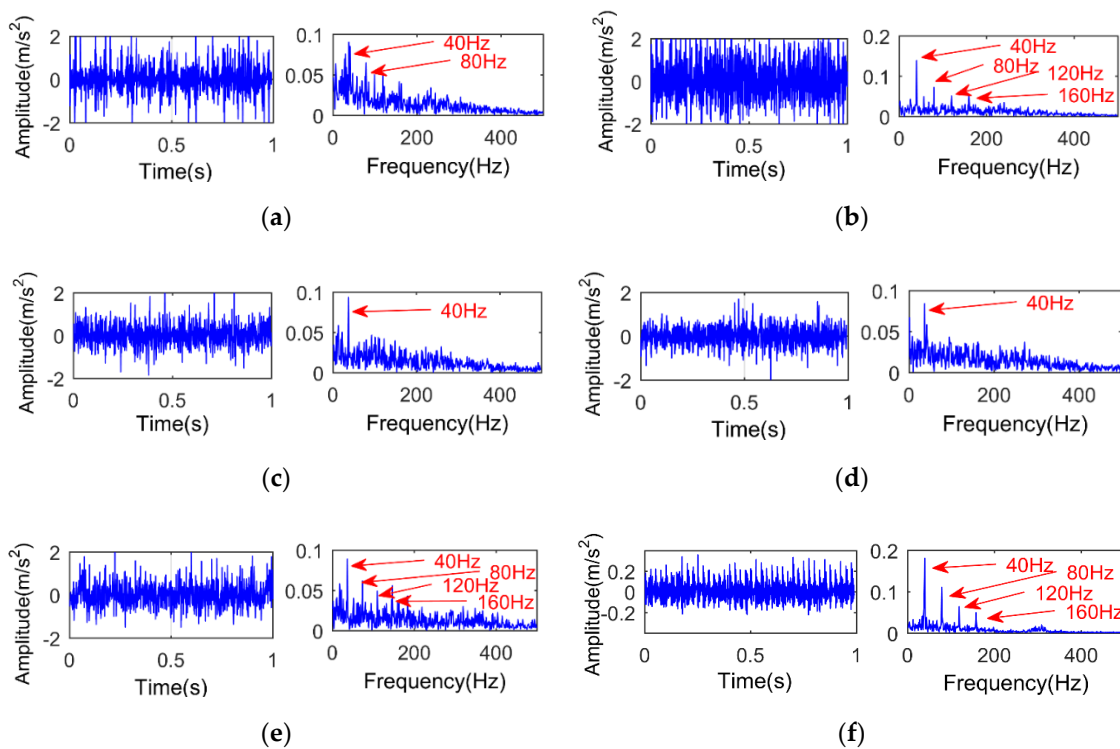


Figure 6. Simulation signals are processed by (a) AR; (b) ARMA; (c) MED; (d) AR-MED; (e) ARMA-MED; (f) ARMA-MOMEDA.

To elaborate on the performance advantages of the proposed method, we use permutation entropy [45] and the fault energy ratio [46] to compare several methods from time to time and across the frequency domain. The comparison results are shown in Table 1.

Table 1. Comparison of simulation results. ARMA, autoregressive moving average; MOMEDA, multipoint optimal minimum entropy deconvolution adjusted.

Method	AR	ARMA	MED	ARMED	ARMAMED	ARMAMOMEDA
Permutation Entropy	4.6870	4.5623	4.7073	4.7069	4.7033	4.3100
Fault Energy Ratio	0.0211	0.03971	0.0263	0.0286	0.02674	0.06707

It can be seen from the results of Table 1 that the permutation entropy value of the proposed method is smaller than that of other methods, which proves that the signal of the simulated signal processed by the method is more regular. By comparing the fault energy ratio, the value of the fault energy ratio of the proposed method is larger than that of the original fault diagnosis method. The performance of the proposed method is proven by the verification of the simulation results by permutation entropy and the fault energy ratio.

5. Experimental Verification

In order to verify the effectiveness of the proposed method in engineering applications, the data of Case Western Reserve University Bearing Data Center were used for experimental verification [47]. The test bench shown in Figure 7 mainly includes a test gearbox, a console, a motor, and a piezoelectric acceleration sensor. The motor has a power of 2 horsepower.

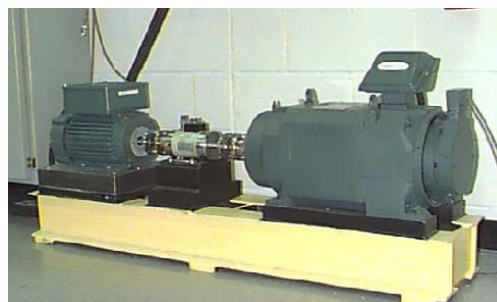


Figure 7. Bearing fault diagnosis test bench.

The fault of the rolling bearing is achieved by machining the inner ring of the bearing with a spark. The bearing type is 6205-2RS JEM SKF (Svenska Kullagerfabriken). During the experiment, the motor speed is 1797 RPM, the sampling frequency is 48,000 Hz, and the sampling point is 4096. The fault frequency can be obtained by calculation, as shown in Table 2.

Table 2. Fault frequency.

Rotation Speed	Rotational Frequency	Fault Frequency of Inter Ring
1797 rpm	30 Hz	162.4 Hz

Figure 8 shows the time-domain diagram and envelope spectrum of the fault signal. It can be seen from the above Figure 8a that the collected vibration signal contains fault information, but the fault information is not clearly located. The envelope spectrum analysis of the time domain signal is shown in Figure 8b, and only one tip pulse is extracted. The fault frequency cannot be accurately described. The vibration signal is processed separately by the traditional MOMEDA and the ARMA-MOMEDA proposed in this paper, and the effects of each method are compared.

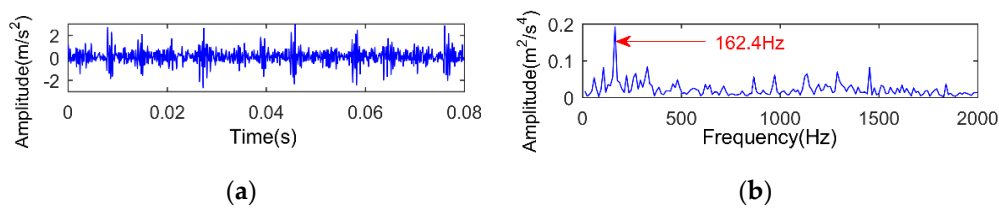


Figure 8. Time domain and envelope spectrum of fault signal. (a) The time-domain diagram; (b) spectral envelope diagram.

5.1. The Analysis Results of MOMEDA

The obtained vibration signal is analyzed by the MOMEDA method, and the obtained analysis result is shown in Figure 9. Figure 9a is a time-domain graph of the analysis result, and Figure 9b is an envelope spectrum graph of the analysis result. It can be seen that the number of effective pulses in the envelope spectrum of the original signal processed by MOMEDA is increased, and the extracted fault frequency is 162.4 Hz. The experimental results were compared by permutation entropy and the fault energy ratio. The results of the comparison between the original experimental signal and the signal processed by MOMEDA are shown in Table 3. It can be seen from the results in Table 3 that permutation entropy of the experimental signal is reduced after MOMEDA processing, which proves that the regularity of the signal increases, and the fault energy ratio of the signal also increases.

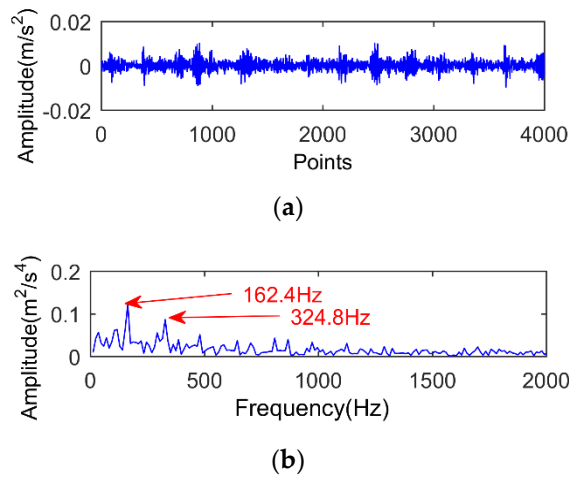


Figure 9. Time domain and envelope spectra of experimental signals. (a) The time-domain diagram; (b) spectral envelope diagram.

Table 3. Comparison of experimental results of MOMEDA.

Method	Original Signal	MOMEDA
Permutation Entropy	4.7653	4.3218
Fault Energy Ratio	0.03658	0.04136

5.2. Decomposition Results of the Method Proposed in this Paper

The signals were analyzed using the method proposed in this paper. First, the collected vibration signal is filtered once by the ARMA filter, and the filtered signal is as shown in Figure 10. Figure 10a is the time-domain signal of the experimental signal, and Figure 10b is the time-domain diagram of the experimental signal after ARMA processing. It can be seen that the amplitude of the noise amplitude of the signal after ARMA filtering has an intuitive drop, and the effective residual signal is retained. This makes the effect of noise on the MOMEDA filter weakened, making the extraction of weak faults more accurate.

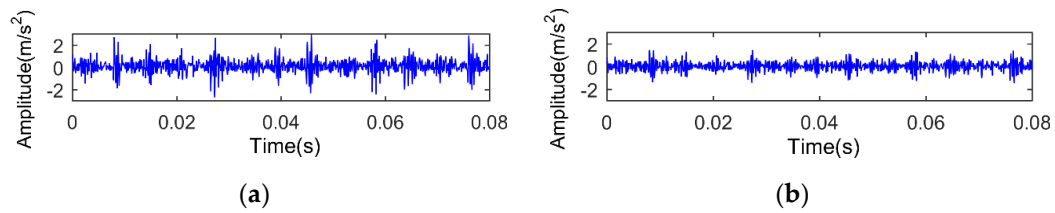


Figure 10. The time-domain comparison diagram of the experimental signal and the signal processed by ARMA. (a) The time-domain diagram of the experimental signal; (b) the time-domain diagram after ARMA processing.

Then, according to the work of [35], the length of filter $L = 200$ is selected in this paper, and the calculated failure frequency is 162.4 Hz, and the corresponding sampling points are 295.5, so the selected filter interval is [220, 24,000]. The MOMEDA algorithm is used to extract the fault features of the ARMA noise-reduced signal. The extraction result is shown in Figure 11. Figure 11a is the time-domain graph of the analysis result, and Figure 11b is the envelope spectrum graph of the analysis result. It can be seen that the amplitude of the time-domain diagram is more obvious after the processing of the method proposed in this paper and five peaks can be clearly highlighted in the envelope spectrum. The extracted fault frequency is 162.4 Hz.

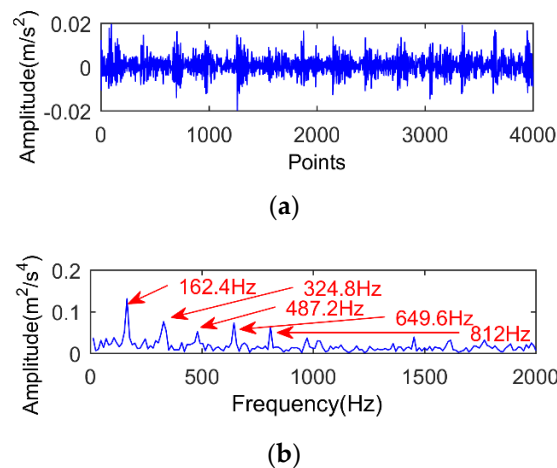


Figure 11. The time-domain and envelope spectrum of the experimental signal processed by ARMA-MOMEDA. (a) The time-domain diagram; (b) spectral envelope diagram.

Compared with the MOMEDA method, the proposed method can extract fault information with higher precision and has better performance in weak fault feature extraction. It can be seen from Table 4 that the value of the permutation entropy of the proposed method is smaller than the that with the MOMEDA method, and the fault energy ratio is larger than the MOMEDA method. It can be seen that, in practical applications, the proposed method is superior to the traditional MOMEDA method.

Table 4. Comparison of experimental results of ARMA-MOMEDA.

Method	MOMEDA	ARMA-MOMEDA
Permutation Entropy	4.3218	4.0362
Fault Energy Ratio	0.04136	0.06536

6. Conclusions

This paper proposes an ARMA-MOMEDA method that was successfully applied to gearbox bearings’ fault diagnosis. The method can extract the weak fault features in the gearbox with higher

precision, and the effectiveness is verified through simulation and experiment. Through simulation and experiment, the following conclusions are drawn:

MOMEDA can extract significant faults, but its extraction effect is easily affected by the noise. In order to promote its weak fault feature extraction performance, it is improved via the following steps. Before processing the collected vibration signal, noise reduction is performed by ARMA, so as to better highlight the fault feature. Then, the fault feature of the vibration signal is extracted by the MOMEDA algorithm. The method extracts the fault feature of the bearing inner ring in the gearbox with high precision. The simulation results and experimental results are verified by the permutation entropy and the fault energy ratio. The method provides a new idea for extracting weak fault features and has a certain reference value.

Author Contributions: J.W. (Junyuan Wang) and Z.W. performed the simulation experiment; J.W. (Jingtai Wang) wrote the paper; W.D. and J.Z. analyzed the data and contributed reagents/materials/analysis tools; G.W. and T.L. revised the paper.

Funding: This work was supported in part by the National Natural Science Foundation of China under Grant 51905496; the Provincial Natural Science Foundation of China under Grant 201801D221237, 201801D121185, 201801D121186, 201801D121187, and 201701D121061; and in part by the Science Foundation of North University of China under Grant XJJ201802.

Conflicts of Interest: The authors declare no conflict of interest.

References

- Li, Y.B.; Yang, Y.T.; Wang, X.Z. Early fault diagnosis of rolling bearings based on hierarchical symbol dynamic entropy and binary tree support vector machine. *J. Sound Vib.* **2018**, *428*, 72–86. [[CrossRef](#)]
- Wang, Z.J.; Han, Z.N.; Gu, F.S. A novel procedure for diagnosing multiple faults in rotating machinery. *ISA Trans.* **2015**, *55*, 208–218. [[CrossRef](#)] [[PubMed](#)]
- Wang, X.; Zhou, F. Weak fault diagnosis of rolling bearing under variable speed condition using IEWT-based enhanced envelope order spectrum. *Meas. Sci. Technol.* **2019**, *30*. [[CrossRef](#)]
- Zhao, M.; Lin, J.; Miao, Y.H. Detection and recovery of fault impulses via improved harmonic product spectrum and its application in defect size estimation of train bearings. *Measurement* **2016**, *91*, 421–439. [[CrossRef](#)]
- Li, Z.; Ma, J.; Wang, X.; Wu, J. MVMD-MOMEDA-TEO Model and Its Application in Feature Extraction for Rolling Bearings. *Entropy* **2019**, *21*, 331. [[CrossRef](#)]
- Zhao, M.; Jia, X.D. A novel strategy for signal denoising using reweighted SVD and its applications to weak fault feature enhancement of rotating machinery. *Mech. Syst. Signal Process.* **2017**, *94*, 129–147. [[CrossRef](#)]
- Kun, Y.; Tian, R. A combined polynomial chirplet transform and synchroextracting technique for analyzing nonstationary signals of rotating machinery. *IEEE Trans. Instrum. Meas.* **2019**, in press. [[CrossRef](#)]
- Wang, X.; Yan, X.; He, Y. Weak Fault Feature Extraction and Enhancement of Wind Turbine Bearing Based on OCYCBD and SVDD. *Appl. Sci.* **2019**, *9*, 3706. [[CrossRef](#)]
- Andrea, F.; Domenico, G.; Domenico, L. Design of Delivery Valve for Hydraulic Pumps. *Machines* **2018**, *6*, 44.
- Francesco, V. On the evaluation of errors in the virtual design of mechanical. *Machines* **2018**, *6*, 36.
- Wang, S.H.; Xiang, J.W.; Zhong, Y.T. A data indicator-based deep belief networks to detect multiple faults in axial piston pumps. *Mech. Syst. Signal Process.* **2018**, *112*, 154–170. [[CrossRef](#)]
- Wang, Y.; Tse, P.W.; Tang, B.P. Kurtogram manifold learning and its application to rolling bearing weak signal detection. *Measurement* **2018**, *127*, 533–545. [[CrossRef](#)]
- Wang, Z.J.; He, G.F.; Du, W.H. Application of Parameter Optimized Variational Mode Decomposition Method in Fault Diagnosis of Gearbox. *IEEE Access* **2019**, *7*, 44871–44882. [[CrossRef](#)]
- Liu, H.; Xiang, J. Kernel regression residual decomposition-based synchro extracting transform to detect faults in mechanical systems. *ISA Trans.* **2019**, *87*, 251–263. [[CrossRef](#)] [[PubMed](#)]
- Wang, Z.J.; Zheng, L.K.; Du, W.H. A novel method for intelligent fault diagnosis of bearing based on capsule neural network. *Complexity* **2019**. [[CrossRef](#)]
- Wang, Z.J.; Zhou, J.; Wang, J.Y. A novel Fault Diagnosis Method of Gearbox Based on Maximum Kurtosis Spectral Entropy Deconvolution. *IEEE Access* **2019**, *7*, 29520–29532. [[CrossRef](#)]

17. Wang, H.Q.; Li, S.; Song, L.Y. A novel convolutional neural network-based fault recognition method via image fusion of multi-vibration-signals. *Comput. Ind.* **2019**, *105*, 182–190. [[CrossRef](#)]
18. Zhou, Y.; Liu, X. An Online Damage Identification Approach for NC Machine Tools Based on Data Fusion Using Vibration Signals. *J. Vib. Control* **2015**, *21*, 2925–2936.
19. Jiang, X.X.; Wang, J. A coarse-to-fine decomposing strategy of VMD for extraction of weak repetitive transients in fault diagnosis of rotating machines. *Mech. Syst. Signal Process.* **2019**, *116*, 668–692. [[CrossRef](#)]
20. Wang, H.; Wang, P.; Song, L. A Novel Feature Enhancement Method based on Improved Constraint Model of Online Dictionary Learning. *IEEE Access* **2019**, *7*, 17599–17607. [[CrossRef](#)]
21. Wang, Y.; Tse, P.W.; Tang, B.P. Order spectrogram visualization for rolling bearing fault detection under speed variation conditions. *Mech. Syst. Signal Process.* **2019**, *122*, 580–596. [[CrossRef](#)]
22. Song, L.Y.; Wang, H.Q.; Chen, P. Step-by-step Fuzzy Diagnosis Method for Equipment Based on Symptom Extraction and Trivalent Logic Fuzzy Diagnosis Theory. *IEEE Trans. Fuzzy Syst.* **2018**, *26*, 3467–3478. [[CrossRef](#)]
23. Li, Y.; Li, G.; Yang, Y. A fault diagnosis scheme for planetary gearboxes using adaptive multi-scale morphology filter and modified hierarchical permutation entropy. *Mech. Syst. Signal Process.* **2018**, *105*, 319–337. [[CrossRef](#)]
24. Yan, X.; Liu, Y.; Jia, M. A Feature Selection Framework-Based Multiscale Morphological Analysis Algorithm for Fault Diagnosis of Rolling Element Bearing. *IEEE Access* **2019**, *7*, 123436–123452. [[CrossRef](#)]
25. Yan, X.; Liu, Y.; Jia, M. Research on an enhanced scale morphological-hat product filtering in incipient fault detection of rolling element bearings. *Measurement* **2019**, *147*, 106856. [[CrossRef](#)]
26. Wang, Z.J.; Zheng, L.K. Research of novel bearing fault diagnosis method based on improved krill herd algorithm and kernel Extreme Learning Machine. *Complexity* **2019**. [[CrossRef](#)]
27. Zheng, J.; Pan, H.; Cheng, J. Rolling bearing fault detection and diagnosis based on composite multiscale fuzzy entropy and ensemble support vector machines. *Mech. Syst. Signal Process.* **2017**, *85*, 296–311. [[CrossRef](#)]
28. Wiggins, R.A. Minimum entropy deconvolution. *Geophys. Prospect. Pet.* **1980**, *16*, 21–35. [[CrossRef](#)]
29. Sawalhi, N.; Randall, R.B.; Endo, H. The enhancement of fault detection and diagnosis in rolling element bearings using minimum entropy deconvolution combined with spectral kurtosis. *Mech. Syst. Signal Process.* **2007**, *21*, 2616–2633. [[CrossRef](#)]
30. Wang, S.; Xiang, J.; Tang, H. Minimum entropy deconvolution based on simulation determined band pass filter to detect faults in bearings of axial piston pumps. *ISA Trans.* **2019**. [[CrossRef](#)]
31. Sprenger, T.; Sperl, J.; Fernandez, B. Bias and precision analysis of diffusional kurtosis imaging for different acquisition schemes. *Magn. Reson. Med.* **2016**, *76*, 1684–1696. [[CrossRef](#)] [[PubMed](#)]
32. McDonald, G.L.; Zhao, Q. Multipoint Optimal Minimum Entropy Deconvolution and Convolution Fix: Application to vibration fault detection. *Mech. Syst. Signal Process.* **2017**, *82*, 461–477. [[CrossRef](#)]
33. Cai, W.; Wang, Z. Application of an Improved Multipoint Optimal Minimum Entropy Deconvolution Adjusted for Gearbox Composite Fault Diagnosis. *Sensors* **2018**, *18*, 2861. [[CrossRef](#)] [[PubMed](#)]
34. Sun, H.; Wu, C.; Liang, X. Identification of Multiple Faults in Gearbox Based on Multipoint Optimal Minimum Entropy Deconvolution Adjusted and Permutation Entropy. *Entropy* **2018**, *20*, 850. [[CrossRef](#)]
35. Wang, Z.; Du, W.; Wang, J. Research and Application of Improved Adaptive MOMEDA Fault Diagnosis Method. *Measurement* **2019**, *140*, 63–75. [[CrossRef](#)]
36. Wang, Z.J.; Wang, J.Y. Application of an Improved Ensemble Local Mean Decomposition Method for Gearbox Composite Fault diagnosis. *Complexity* **2019**. [[CrossRef](#)]
37. Xu, Y.; Cai, Z.; Cai, X. An enhanced multipoint optimal minimum entropy deconvolution approach for bearing fault detection of spur gearbox. *J. Mech. Sci. Technol.* **2019**, *33*, 2573–2586. [[CrossRef](#)]
38. Jiang, X.; Cheng, X.; Shi, J.; Huang, W. A new $l(0)$ -norm embedded MED method for roller element bearing fault diagnosis at early stage of damage. *Measurement* **2018**, *127*, 414–424. [[CrossRef](#)]
39. Takalo, R.; Hytti, H.; Ihalaine, H. Adaptive Autoregressive Model for Reduction of Noise in SPECT. *Comput. Math. Methods Med.* **2015**, *2015*, 494691. [[CrossRef](#)]
40. Endo, H.; Randall, R.B. Enhancement of autoregressive model-based gear tooth fault detection technique by the use of minimum entropy deconvolution filter. *Mech. Syst. Signal Process.* **2007**, *21*, 906–919. [[CrossRef](#)]

41. Li, Q.; Ji, X.; Liang, S. Incipient Fault Feature Extraction for Rotating Machinery Based on Improved AR-Minimum Entropy Deconvolution Combined with Variational Mode Decomposition Approach. *Entropy* **2017**, *19*, 317. [[CrossRef](#)]
42. Gao, S.; Li, B. Study on Slurry Noise of Electromagnetic Flowmeter Based on ARMA Power Spectrum Estimation. *Math. Probl. Eng.* **2015**, *2015*, 976487. [[CrossRef](#)]
43. Cong, F.; Chen, J.; Dong, G. Spectral kurtosis based on AR model for fault diagnosis and condition monitoring of rolling bearing. *J. Mech. Sci. Technol.* **2012**, *26*, 301–306. [[CrossRef](#)]
44. Wang, L.; Pan, J. Incipient fault diagnosis of limit switch based on a ARMA model. *Measurement* **2019**, *135*, 473–480. [[CrossRef](#)]
45. Zhou, J.; Guo, X. Research on fault extraction method of variational mode decomposition based on immunized fruit fly optimization algorithm. *Entropy* **2019**, *21*, 400. [[CrossRef](#)]
46. Wan, S.; Peng, B. The FERgram: A rolling bearing compound fault diagnosis based on maximal overlap discrete wavelet packet transform and fault energy ratio. *J. Mech. Sci. Technol.* **2019**, *33*, 157–172. [[CrossRef](#)]
47. Li, Y.; Wang, X.; Si, S.; Huang, S. Entropy based fault classification using the Case Western Reserve University data a benchmark study. *IEEE Trans. Reliab.* **2019**, 1–14. [[CrossRef](#)]



© 2019 by the authors. Licensee MDPI, Basel, Switzerland. This article is an open access article distributed under the terms and conditions of the Creative Commons Attribution (CC BY) license (<http://creativecommons.org/licenses/by/4.0/>).